Free-Neutron Beta-Decay Half-Life

C. J. Christensen, A. Nielsen,* A. Bahnsen,† W. K. Brown,‡ and B. M. Rustad§
Danish Atomic Energy Commission, Research Establishment Risö, Physics Department, Roskilde, Denmark
(Received 4 November 1971)

The β-decay half-life of the free neutron was measured. Greater accuracy was obtained through the development of a special 4π β spectrometer with a well-defined source volume and through the use of a new density calibration method with a ^{3}He proportional counter. A clean thermal-neutron beam was developed especially for the measurement. The final result is a half-life of 10.61 ± 0.16 min. The derived value of g_A/g_V is -1.239 ± 0.011.

I. INTRODUCTION

The importance of precision knowledge of the radioactive half-life of the neutron is akin to that of the fundamental constants. Measurements of this quantity are clearly of central importance to β-decay theory,[1] and have far-reaching effects in astrophysics and cosmology.[2]

An over-all review of the subject is contained in an article by Kofoed-Hansen and Christensen published in 1962.[1] Table I summarizes the results over the years (Refs. 3–11).

We have remeasured the neutron half-life. A preliminary result was published in 1967.[11] Below the final results are presented along with a summary of the essential ingredients of the experiments. The improved accuracy was achieved with a carefully designed low-background beam facility in the DR 3 heavy-water-moderated reactor,[12,13] with a newly developed precision beam calibration,[14] and with a 4π magnetic β spectrometer described herein.

Many details have been omitted in this presentation. The reader is referred to a more comprehensive description in an unpublished report[15] for such details.

II. GENERAL DESCRIPTION OF THE MEASUREMENT

The method used for our measurement of the neutron half-life is conceptually simple and generally similar to that used previously by Snell *et al.*,[5] Robson,[8] and Sosnovsky *et al.*[10] If in a known volume V of a thermal-neutron beam the neutron density $n(\vec{r})$ is known at every point $\vec{r}$, and the neutron-decay count rate C_d is measured by means of a detector that subtends the known geometrical efficiency (solid angle) $\Omega(\vec{r})$ and has a known intrinsic efficiency $\epsilon(\vec{r})$, then

$$C_d = \lambda \int_V n(\vec{r}) \frac{\Omega(\vec{r})}{4\pi} \epsilon(\vec{r})\, d^3r = \frac{\ln 2}{T_{1/2}} N \frac{\langle \epsilon\Omega \rangle}{4\pi} . \quad (1)$$

Thus the decay probability λ (or the half-life $T_{1/2}$) is expressed in terms of C_d, the number of neutrons N within the source volume V, and a suitable average $\langle \epsilon\Omega \rangle$ of $\epsilon\Omega$ over the source volume:

$$N\langle \epsilon\Omega \rangle \equiv \int_V n(\vec{r})\Omega(\vec{r})\epsilon(\vec{r})\, d^3r . \quad (2)$$

The major experimental problem is the difficulty in accurately defining the source volume and the solid angle subtended by the detector. Our solution to this problem was the development of a 4π β spectrometer through which the neutron beam passes. Figure 1 helps visualize this 4π β spectrometer. A homogeneous magnetic field of 0.7 Wb/m^2 is set up vertically across the horizontal neutron beam. β particles from neutron decays are then constrained to follow helical paths up or down along the magnetic field lines. Placed above and below the beam for detection of the β's are flat scintillator plates of identical shape – thick enough to stop the most energetic β's from neutron decays. The magnetic field holds even these maximum-energy electrons to helices of radii that are much smaller than the length and width of the detectors. Thus to a good approximation the sensitive volume can be visualized as a rectangular "box," having the two scintillators as top and bottom, and having as sides those field lines that join the edges of the scintillators. The beam passes through this box parallel to the longest sides of the scintillators and centered between them. The beam diameter in the box (2.5 cm) is so much smaller than the width of the box that from nowhere in the beam can decay electrons spiral past the sides of the scintillators. Therefore the source volume is the total volume of the beam that is limited by two planes (perpendicular to the beam and defined by the ends of the scintillators).

The most essential features of the spectrometer are the following: The source volume is well defined except for a region of thickness 4ρ (ρ is the helix radius) around the ends of the sensitive box (Sec. III E). The geometrical efficiency ($\Omega/4\pi$) is

TABLE I. Summary of neutron half-life measurements.

Experimenters	Reference	Value quoted (min)
Snell and Miller	3	15–30
Robson	4	9–18
Snell, Pleasonton, and McCord	5	10–30
Robson	6	9–25
Spivak *et al.*	7	8–15
Robson	8	12.8 ±2.5
Spivak *et al.*	7	12 ±1.5
D'Angelo	9	12.7 ±1.9
Sosnovsky *et al.*	10	11.7 ±0.3
Christensen *et al.* (preliminary)	11	10.78±0.16
Present final result		10.61±0.16

unity everywhere in the source volume except for a small correction due to a sideways drift of electrons whose velocity is nearly perpendicular to the field (Sec. III D). The intrinsic efficiency $\epsilon(\vec{r})$ (which is really also a function of the discriminator level, see Sec. III B) is independent of $\vec{r}$ because of the homogeneity of the scintillators (Sec. III E). Finally, the problem of spectrum distortion due to backscattering of electrons is eliminated because the magnetic field will force backscattered electrons to hit the other detector (Sec. III B).

Background effects are a serious problem. The scintillators are very sensitive to γ's and fast neutrons, and the background pulses from these are indistinguishable from those of decay electrons – except for their energy spectrum. This necessitates a spectrometer rather than a simple β detector. The measured decay spectra are corrected for background with the combined use of two sets of shutters. A pair of aluminum plates can be inserted between the beam and the two detectors to stop neutron-decay β's, and a $^6Li_2CO_3$ thermal-neutron beam stopper can be inserted in the beam (see Fig. 1 and Sec. IV).

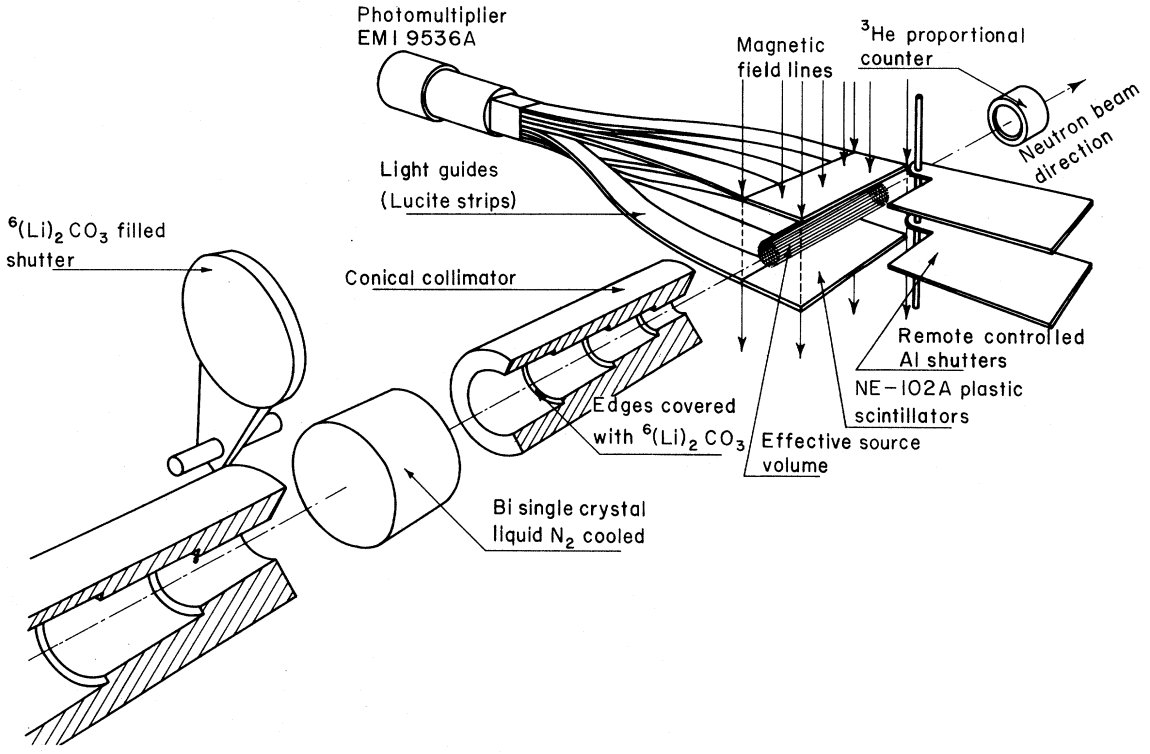

FIG. 1. Diagram of the Risö neutron half-life measurement equipment showing the β spectrometer and the source volume definition.

We measured the number of neutrons present in the source volume by means of a thin ^{3}He proportional counter (Sec. V) that has plane, parallel walls (perpendicular to the beam) and accepts the total beam cross section.

Thus the source volume for neutron decays and the source volume for $^3\mathrm{He}(n,p)^3\mathrm{T}$ reactions are of very similar geometrical characteristics, i.e., right circular cylinders of the same cross section as the total beam, and of well-defined lengths (L and T, respectively), and both are $1/v$ neutron detectors.

Therefore the ratio between the neutron-decay count rate and the ^{3}He-counter count rate is[15]

$$\frac{C_d}{C_n}=\frac{\epsilon(\Omega/4\pi)\lambda L}{\rho_{\mathrm{He}}\sigma_0 v_0 T}=\frac{\ln 2\,\epsilon(\Omega/4\pi)L}{T_{1/2}\rho_{\mathrm{He}}\sigma_0 v_0 T}\,, \tag{3}$$

where σ_0 is the cross section for the ^{3}He reaction at the neutron velocity $v_0 = 2\,200$ m/sec and ρ_{He} is the ^{3}He density. Even though this basic equation allows us to carry through the analysis of the experiment without reference to the neutron density or current, we have found it convenient to introduce a symbol n_z (the linear neutron density, in units of neutrons per unit length of the total beam of cross section S)

$$n_z \equiv \int_S d^2r\, n(\vec{\mathbf{r}}) \quad \left[=\int dv\, n_z(v)=\int dv \int_S d^2r\, n(\vec{\mathbf{r}},v)\right], \tag{4}$$

where $n(\vec{\mathbf{r}},v)$ is the usual neutron-density velocity distribution and $n_z(v)$ is defined as shown in Eq. (4).

III. NEUTRON BETA-DECAY SPECTROMETER

Presented below are details of the 4π β spectrometer which was described in general in conjunction with Fig. 1.

A. Hardware

The β detection system (see Fig. 1) is mounted inside a stainless-steel vacuum chamber which itself is an integral part of the neutron beam tube. The two identical β detectors are flat plates of NE 102A scintillating plastic,[16] each 5×10×0.32 cm. The plates are positioned horizontally, 9 cm above and below the beam center line, respectively. The gross-fiber-optics light-guide system optically adds scintillations from the two detectors into a single 2-in. photomultiplier tube (EMI 9536A).

The spectrometer is placed in the center of a vertical magnetic field. The flat pole pieces of the magnet are 60 cm in diameter with a gap of 35 cm. This configuration gives a reasonably homogeneous field between the two detectors.

B. Spectral Response and Efficiency

Our 4π β spectrometer is used for measuring the β spectrum shape and the absolute source strength. In order to do this it is of critical importance to know the response function of the spectrometer. The shape of the measured spectrum is not the shape of the true β spectrum, but rather its convolution with the response function $R(E,E')$:

$$P_{\mathrm{exp}}(E')dE' = dE' \int_0^\infty R(E,E')P_{\mathrm{th}}(E)dE\,. \tag{5}$$

Here $P_{\mathrm{th}}(E)dE$ is the theoretical β spectrum, and $P_{\mathrm{exp}}(E')dE'$ is the measured shape. The function $R(E,E')\,dE'$ is the spectrometer response, i.e., the pulse-height (E') spectrum resulting from monoenergetic electrons of energy E.

For the measurement of the absolute source strength it is necessary to use only pulses higher than a chosen discriminator level E_d' (in terms of electron energy chosen to be $0.4mc^2$ or 204 keV) in order to minimize the background effects which rise sharply at lower energies. As a consequence the intrinsic efficiency is lower than 100%, and must be accurately determined.

If $P_{\mathrm{exp}}(E')$, $P_{\mathrm{th}}(E)$, and $R(E,E')$ are properly normalized, the efficiency ϵ will be

$$\epsilon(E_d') = \int_{E_d'}^\infty P_{\mathrm{exp}}(E')\,dE' = \int_{E_d'}^\infty dE' \int_0^\infty R(E,E')P_{\mathrm{th}}(E)\,dE\,. \tag{6}$$

Thus if $R(E,E')$ and $P_{\mathrm{th}}(E)$ are well enough known, the expected shapes of the measured spectra can be calculated and compared with the measured spectra, and the efficiency can be calculated from the above expressions.

The procedures for determining $R(E,E')$ are described in detail in Ref. 15. The main results are as follows. For a system like ours one expects the response function to be a Poissonian. Mathematically it can be represented by the expression

$$R(E,E')\,dE' = \frac{[K(E-E_0)]^{K(E'-E_0)}}{[K(E'-E_0)]!}\,e^{-K(E-E_0)}d(KE')\,. \tag{7}$$

K and E_0 are adjustable parameters: K is the average number of photoelectrons per unit energy produced in the photocathode, and E_0 accounts for a low-energy cutoff in the pulse height versus energy relationship.

K and E_0 were determined experimentally, and the response function was verified by measuring the responses for a series of internal conversion electron line sources.

Figure 2 shows the recorded spectra for several

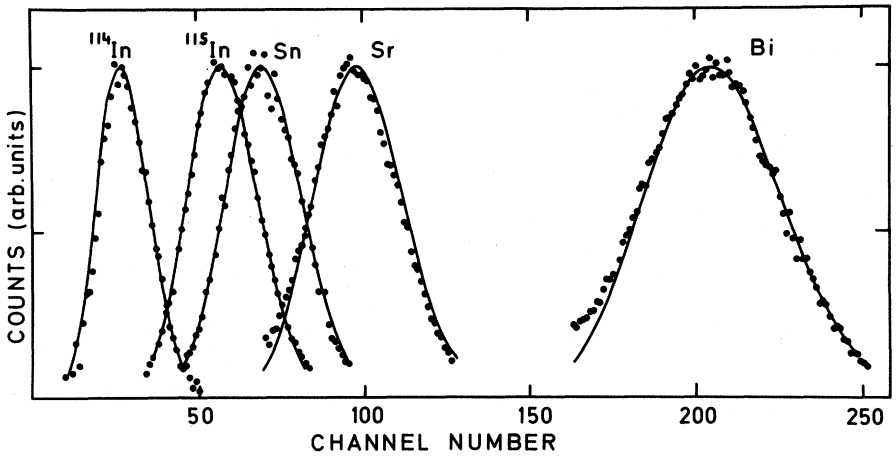

FIG. 2. A series of electron spectra from In^{114}, In^{115}, Sn^{113}, Sr^{85}, and Bi^{207}. Analysis yields the response function and the calibration of the β spectrometer. The data have been fitted with a resolution-broadened Poissonian distribution, as described in the text.

of these sources. Also shown are response curves calculated from Eq. (7) for the best values of K and E_0 (i.e., $K=120$ photoelectrons/MeV and $E_0=40$ keV). The assumed $R(E, E')$ is seen to represent the lines quite well.

Figure 3 shows a plot of the average channel number for the peaks versus the electron energy for two different gain settings. Figures 2 and 3 show small deviations from linearity in the position of the peaks. This has two causes: First, Auger-electron emission, together with a lack of knowledge of the response for very low-energy electrons (<50 keV), introduces an uncertainty in the energy assigned to the primary electrons from the sources. Secondly, the scatter of the points in the Fig. 3-type plot was slightly different from time to time. This is presumably due to minor drifts caused by the introduction and removal of sources, and to the statistics in each single line position.

As discussed in Ref. 15 it should be added that the fit of $R(E, E')$ to the electron line sources adds support to our claim that the dual detector geometry eliminates the problem of backscattering of electrons and therefore eliminates any tail on the low-energy side of the lines.

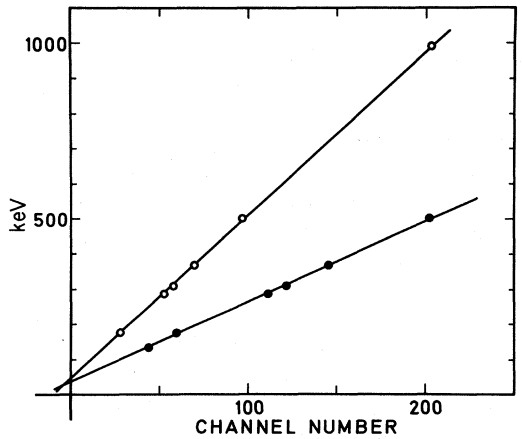

FIG. 3. An energy calibration of the β spectrometer.

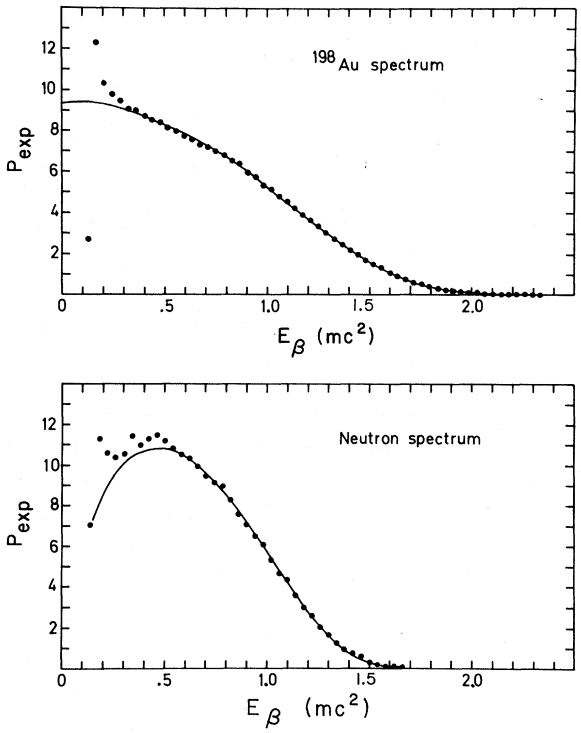

FIG. 4. Gold and neutron β-decay spectra measured with the β spectrometer. The solid lines have been generated by folding the theoretical spectra with the spectrometer resolution function.

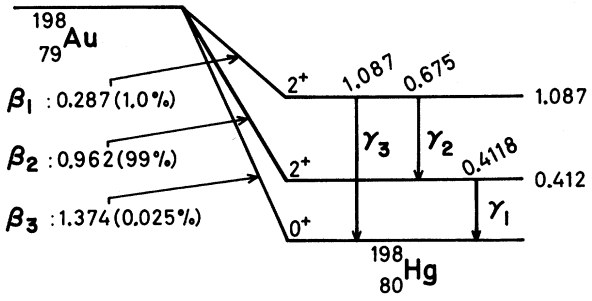

FIG. 5. The β-decay scheme of ^{198}Au.

When the detailed shape of $R(E, E')$ has been established, it is easy to calculate the efficiency for the particular β spectrum being studied [Eq. (6)]. For the neutron decay we found $\epsilon = 0.68$ for $E_d' = 0.4mc^2$. To account for the scatter in the points of Fig. 3 we assign a statistical uncertainty of $\pm 1\%$ to ϵ. This corresponds to ± 3.5-keV uncertainty in E_d'. This uncertainty is statistical insofar as the error is different for different calibrations and it agrees with our experience from many absolute measurements of ^{198}Au (see Sec. III C). In addition we assume that this calculated ϵ may be lower than the real ϵ by $(0.5 \pm 0.5)\%$ because of systematic errors arising from slight nonlinearities of the system. This makes the half-life too low when the calculated ϵ is used.

For the calculation of the anticipated experimental β spectrum from neutron decay, the statistical shape was used. (The Coulomb correction is negligible.) This shape has been verified experimentally by Robson.[8] Figure 4 shows our measured neutron-decay β spectrum, along with the resolution-folded theoretical spectrum. The fit is good above $0.4mc^2$. This verifies that the observed spectrum was indeed that of neutron decay.

C. Verification of Response with ^{198}Au

It was of critical importance to verify the response function folding and efficiency determination procedures to ensure that our understanding of the spectrometer was sufficient to measure neutron decay. A ^{198}Au source, placed in the center of the spectrometer, was used to check both. The

TABLE II. Comparison of ^{198}Au source strengths obtained with the 4π β spectrometer and with the 4π β-γ coincidence counting facility in a typical intercomparison.

	$4\pi\beta$	$4\pi\beta$-γ
	3564	
	3634	
	3614	
Average	3604 ± 21	3588 ± 18

TABLE III. Results of intercomparisons between the Risö 4π β-γ coincidence counting facility and NBS data.

	NBS	Risö 4π β-γ
Thin source	3627	3643 ± 18
Thick source	2234	2230 ± 11

^{198}Au spectrum has a maximum energy of 962 keV (compared with 782.3 keV for the neutron), an almost statistical shape, and a relatively simple decay scheme (Fig. 5).

For the calculation of the β spectrum the following effects were included: The Fermi function was taken from the NBS tables.[17] A shape factor, $S(E) = 1 - 0.33E + 0.074E^2$ (E in mc^2), was applied as inferred from Hamilton's studies of the ^{198}Au spectrum.[18] As the spectrometer detects all β's, three spectral contributions were summed to obtain the theoretical shape: (1) the main 962-keV β spectrum, (2) the weak (1%) $E_{max} = 287$-keV β spectrum, and (3) the 962-keV spectrum shifted up in energy by $(E_\gamma - E_B) = (412 - 83) = 329$ keV because of an internal-conversion (K) electron emitted simultaneously with the main β (and a very small similar L-electron contribution). The contribution of this shifted spectrum relative to the main spectrum was determined from the conversion coefficient $\alpha_K = 0.0282$. The β_3 ground-state transition is negligible.

A sample ^{198}Au spectrum from the spectrometer is shown in Fig. 4, along with the calculated spectrum for comparison. The fit is quite good, except at the low-energy end where some deviation was expected on account of background, low-energy nonlinearity, and energy loss in the source.

Except for the difference in spectra and source volume, the determination of the spectrometer efficiency for ^{198}Au followed procedures identical to those used in the neutron decay rate measurements.

The measured total count rate was compared with a precision activity determination from the Risö 4π β-γ coincidence counting facility. Using the apparatus developed by Thomas and Løvborg,[19] we sandwiched a small flow counter between two scintillation counters and then followed a standard measurement procedure. Table II shows the agreement obtained in the two activity determinations.

In addition, an intercalibration was arranged with Garfinkel[20] of the National Bureau of Standards in Washington, D. C. The activities of both the thin sources discussed in this section and the thick sources of 20 mg/cm^2 used for the ^{3}He-counter development[21] were measured at NBS in a

calibrated γ-scintillation well counter, and at Risö with the 4π β-γ setup. The results are seen in Table III.

These intercomparisons show that: (1) NBS and the Risö 4π β-γ system agree well, although the NBS method is slightly less accurate, and (2) the 4π β counter and the 4π β-γ system agree within the stated uncertainties, i.e., a statistical uncertainty of ±1% (standard deviation of the results of several repeated energy calibrations and source strength measurements, see example in Table II) and a possible systematic error making the 4π β result of Table II too high by (0.5 ± 0.5)% (discussed in Sec. III B).

It is relevant to note that with ^{198}Au, the 4π β-γ coincidence counting system provided a precise check not only on the decay rate measured with the magnetic 4π β spectrometer, but also on the neutron beam density measured with the ^{3}He proportional counter.[14,21] The excellent internal consistency of this double check is extremely valuable, because the neutron half-life is determined from the ratio of the decay rate and beam density measurements.

D. Solid Angle: Magnetic-Mirror and Electron-Drift Effects

The vertical magnetic field actually obtained displayed a small degree of inhomogeneity. With circular, plane-parallel pole pieces, the field lines bulge slightly with azimuthal symmetry. The field is weaker in the center of the gap than at the position of the counters. The difference was measured to be (1.1 ± 0.2)%.

This variation introduces two corrections. The first of these corrections, the increase in effective length due to the bulging field, is discussed in Sec. III E. The second is due to a more complex effect. The electrons are created near the center plane, i.e., in the weaker field. The bulging magnetic field forms a double magnetic mirror that may prevent electrons with a momentum nearly perpendicular to the field from reaching the counters.[22-24] For relevant formulas see, for example, Sivukhin.[25]

Under the conditions of the present experiment, it is calculated that (10.5 ± 1)% of the electrons at any energy will be trapped by the field and will repeatedly spiral up and down the field lines without reaching the detectors. Eventually, the electrons will be scattered by the residual gas molecules, and will escape the solid angle within which they are trapped. The escape must occur in a nuclear scattering event and, on the average, after passage through approximately 0.5 mg/cm^2 of air. At the low pressure in our β chamber (~10^{-5} Torr) this means that the electrons must cycle up and down in the mirror many times. During this time the magnetic field gradient imposes a sideways drift movement on the electrons, in the direction $\vec{\nabla}B\times\vec{B}$. In an axially symmetric field such as ours the drift is in a horizontal circle around the center. This, in turn, means that β's from events near the ends of the source volume may not be detected, because part of the circle along which the electrons drift is outside the source volume. Consequently, if the nuclear scattering event that allows the electrons to escape the mirror occurs to one side or the other of the scintillator plates, the β's will miss the plates.

While spiralling up and down, prior to the nuclear scattering event that allows the escape, the electron will experience electronic scattering and thereby lose some energy. The necessary thickness traversed (0.5 mg/cm^2) should mean a negligible influence on the spectrum because of this scattering. This point was checked in the following way. A small auxiliary coil (15-cm diameter) was placed in the center of the β spectrometer. This coil could boost the magnetic field either to ensure maximum field at the source or make the minimum even more pronounced. ^{198}Au spectra were measured for maximum and minimum fields. No difference could be seen.

The description of electron movement as a combination of the Larmor effect, the up-and-down cycling, and the slow circular drift in the horizontal plane allows a simple correction: Because the electrons are trapped for approximately 100 to 300 drift periods, the detection probability is the average fraction of time the trapped electrons spend inside the source volume. Calculated in this way, the loss is (23 ± 5)% of the trapped electrons, or (2.4 ± 0.6)% of all electrons. This effect was not taken into account in the preliminary report of the experiment,[11] but is included here through adjustment of the geometrical efficiency, $\Omega/4\pi$.

E. Extended Sources

Because the neutron beam constitutes a source extending over the total length of the detectors, the variation in response over the source volume is important. Several effects are significant in this respect.

The gross-fiber-optics principle was used in order to obtain good homogeneity of response. Experience showed this construction to be the best with its high degree of geometric similarity for all possible paths of scintillation light quanta. The peaks of a movable ^{207}Bi source shifted by no more than 2% at any location within the source volume. In spite of this good homogeneity the effect of the

ends of the source volume needs special consideration. Because of the finite electron helix diameter (up to 1.1 cm) the ends are not sharply defined. The solid angle subtended by the detectors for points close to the ends varies gradually from zero at one helix diameter outside the end to unity at one helix diameter inside the end. Electrons from anywhere in these end regions may or may not spiral past the detectors. If the detectors were very thin and the field lines were straight, electrons from the inside which are lost would be exactly compensated by electrons from the outside spiralling in onto the detectors. Thus the effective length would still be equal to the physical length of the scintillators regardless of the finite spiral radius. However, as the electron helix will follow along even a bent field line, the inhomogeneity of the magnetic field will cause a slight increase in source volume length. Also, the finite thickness of the scintillators causes a slight increase of the length because some electrons that should miss the detector will hit its end. These effects are discussed in more detail in Ref. 15.

The effective length was measured in the following way: A rectangular ^{198}Au source, 1×2 cm (along and across the beam, respectively) was moved horizontally through the spectrometer along the beam center line in 1 cm increments to well beyond each end of the sensitive volume, and counted in each position for the same length of time. When the spectra from each position are summed, the result is as if a beam were present

$$L = \frac{\sum \text{counts in all positions}}{\text{counts in center position}} \tag{8}$$

The effective length, inferred from this "equivalent beam" method (for $E_d' = 0.4mc^2$), was 10.25 ±0.05 cm, and is the length used for the half-life determination.

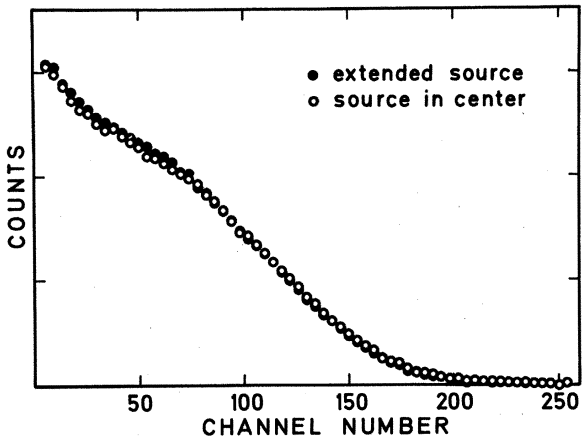

FIG. 6. Comparison of ^{198}Au spectra from both small and extended sources.

The same measurement also gave an idea of the spectral distortion to be expected from the ends. Figure 6 compares ^{198}Au spectra from small and extended sources; note again that the distortion is minimal, and that the main part of it is at the low-energy end.

IV. RADIATION BACKGROUND

The background must be suppressed to such a degree that above some fairly low β energy, the integrated background count rate would be no larger than the β detection rate above that energy. The lower this energy could be pushed, the more accurately the extrapolation of the β spectrum could be made and the total β decay rate determined.

The required performance was obtained from the carefully constructed beam facility.[12,13] Figure 7 shows the complete experimental setup, including the shielding of the different components. Here, only the essential features are mentioned: The beam is obtained from a tangential horizontal beam tube of the heavy-water-moderated DR 3 reactor (thermal flux 5×10^{13} n/cm^2 sec). A thin (2 mm) water scatterer (light water) is placed in the center of the beam tube close to the reactor core. The beam tube is situated in the heavy-water reflector and provides a favorable thermal/fast flux ratio. A conical collimator views the water scatterer exclusively. Halfway down this collimator, a liquid-nitrogen-cooled bismuth single-crystal filter, 32 cm long, filters the beam. This improves the ratio of thermal neutrons to γ's and fast neutrons considerably. The last meter of the collimator leading to the exit orifice is made in such a way that all parts exposed to the direct beam are made of $^6Li_2CO_3$. Slow neutrons removed from the edges of the beam are therefore captured in the γ-free, $^6\text{Li}(n, \alpha)\,^3\text{T}$ reaction.

With this design we obtained a linear neutron density [n_x of Eq. (4)] of roughly 500 n/cm (corresponding to a neutron current of ~6×10^7 n/sec in the total beam at an average neutron velocity of ~1100 m/sec). Typical background rates are shown in Table IV.

The sources of background are manifold, but they may be grouped into two categories: room background and beam-associated background. In order to correct for the background two types of shutters were used (see Fig. 1): the ^{6}Li plate installed near the Bi filter to shut off the beam, and the two aluminum plates which can be inserted between the beam and the scintillators to stop neutron-decay β's. The largest component of the background is the room background. This compo-

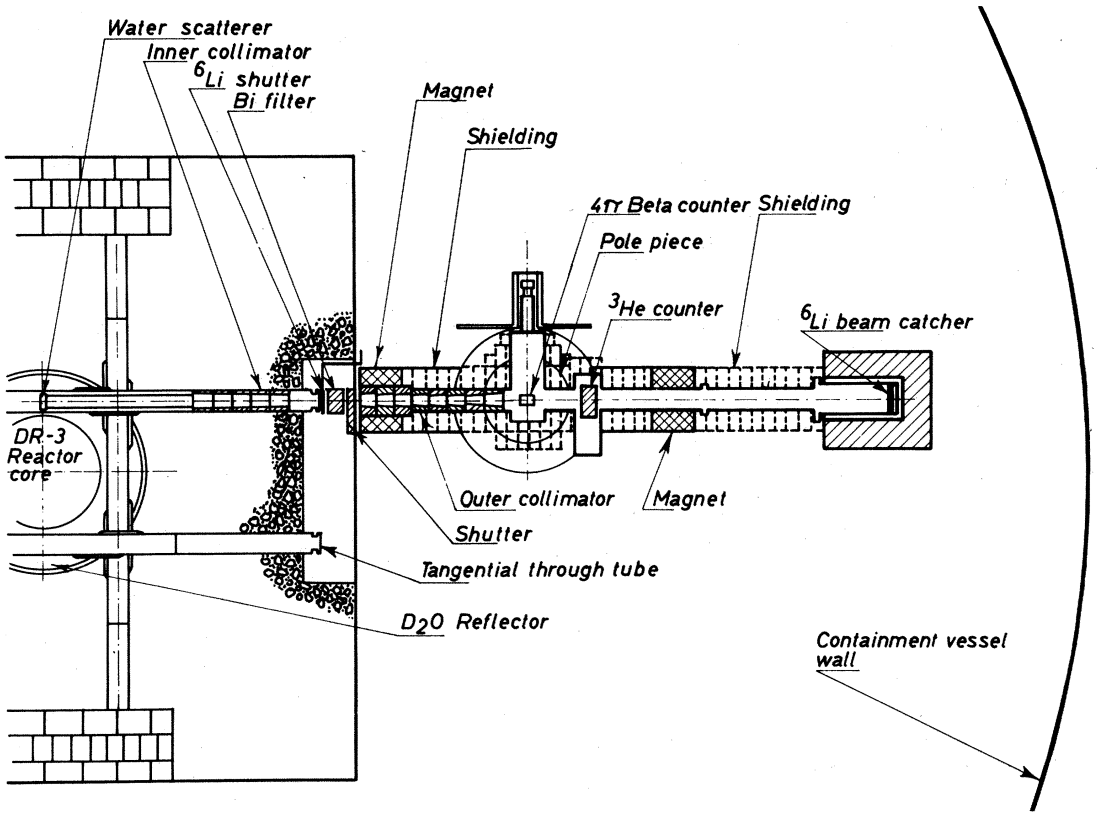

FIG. 7. Top-view diagram of the apparatus showing shielding used in background suppression.

nent originates outside our beam facility and is not influenced by the ^{6}Li shutter. It can therefore be exactly corrected for by a beam-on–beam-off experiment. This same measurement will only partly correct for the beam-associated background. γ's and neutrons coming from the reactor through our collimator and consequently being scattered into the detectors are influenced slightly by the ^{6}Li shutter and thus not corrected for completely. The same is true for capture γ's produced in the collimator walls. Neither can the Al shutters alone correct exactly for background, as they introduce changes in all components of background.

However, in Ref. 15 it was shown that if measurements are made in all four modes (A, B, C, and D, i.e., combinations of ^{6}Li shutter in and out and Al shutters in and out) and the results are combined properly, the background is corrected for sufficiently well. The proper combination of the four modes has the following effects: With the Al shutters out (open) a beam-on–beam-off experiment ($A-C$) yields the neutron-decay count rate, corrected for room background but in error by approximately 5%, essentially due to the total count rate for neutron capture γ's (B_{cap}). These are shut off by the ^{6}Li shutter along with the neutron decays and therefore not corrected for at all. Now another beam-on–beam-off experiment ($B-D$) is made with the Al shutters in (closed). When this ($B-D$) is subtracted from the above ($A-C$) we are left with a corrected result, in error only because of the influence of the Al shutters on the beam associated neutron capture background. The contribution of this and other possible background effects has been calculated in Ref. 15 and is here applied as a correction to the neutron decay rate. The result is that ($B-D$) is higher than the true capture-γ background (i.e., the half-life is too high) by $(1.1\pm0.8)\%$. Minimizing this beam associated background was the main guideline in the

TABLE IV. Count-rate contributions in β spectrometer with discriminator setting equivalent to $\sim 0.4mc^2$.

Contribution	Symbol	Count rate (counts/sec)
Neutron-decay rate	C_T	5
Decay count rate in spectrometer (ϵC_T)	C_d	3.5
Room background	R	5
Beam background, γ+fast n	$B_{\gamma n}$	0.5
Beam background, capture	B_{cap}	0.2

design of the beam facility.

V. NEUTRON-DENSITY MEASUREMENT

The precision standardization of thermal neutron beam intensities has been studied extensively over a period of several years at the Risö laboratory.[26] These studies were initiated and guided partly by the stringent requirements imposed by the neutron half-life measurement. One result of the studies was the construction of a large-area ^{3}He proportional counter with which the neutron density was measured in the present experiment. This counter is described in Refs. 14 and 27.

Besides the ^{3}He-counter method, the gold-foil activation technique for measuring beam density was refined and used to check the ^{3}He measurements.[21] The essential features of the ^{3}He-counter concepts and of the ^{3}He-gold intercomparisons are described in Refs. 14 and 21.

The agreement obtained in the many comparisons with gold in the same beam gave confidence that when the several small corrections to the ^{3}He-detector count rate were made, the beam density could be measured with an accuracy of 0.4%.[14]

The count rate of this counter, C_n, is given by

$$C_n = n_z \rho_{\mathrm{He}} T \sigma_0 v_0 f , \tag{9}$$

where ρ_{He} is the ^{3}He density in atoms/cm^3 within the counter, T is the average thickness of the counter in the beam direction (essentially equal to the physical thickness of the counter, as the windows are flat), and where σ_0 is the $^3\mathrm{He}(n,p)^3T$ cross section at the standard neutron velocity v_0 as given in Ref. 28:

$$\sigma_0 = 5327^{+10}_{-9} \text{ at } v_0 = 2200 \text{ m/sec} .$$

Also, the various small corrections included in the factor f (~1) are discussed in Ref. 14.

Because the ^{3}He counter accepts the entire beam, the fundamental quantity measured is the linear density, n_z (Sec. II). It is clear that although the neutron-density measurement is made downstream from the β spectrometer in the neutron beam, the linear density does not change in between. No material is present which can intercept or attenuate the beam by absorption or scattering except for the ^{3}He-counter windows, which were corrected for (by the factor f included in the equation for the neutron density shown above).

The density measurement was made periodically in a cyclic mode along with the other modes of measurement used to determine the β decay rate. The ^{3}He counter was inserted into the beam only during the density measurements.

In order that unwanted nonstatistical variations (reactor power fluctuations, difficulties with the Bi-filter cooling, etc.) might not be overlooked, the neutron beam was continuously monitored with a ^{235}U-fission proportional counter. The monitor was mounted in a position just downstream from the Bi filter, i.e., sufficiently far back in the collimator to be shielded well enough so as not to introduce capture-γ background in the β decay rate measurements.

However, the final neutron densities used in the half-life determinations were obtained with the ^{3}He counter only. Although any single measurement of density – as mentioned above – could be made with 0.4% accuracy (~0.1% statistical error), the sampling procedure introduced a statistical error in the average neutron density to be used. Each half-life run consisted of ~20 beam-density measurements interspersed with the decay measurements. With fluctuations of the order of ±2% (standard deviation) a statistical accuracy of about $\pm 2/\sqrt{20} = \pm 0.5\%$ in the average density of each run was obtained. For each measurement run this statistical uncertainty was evaluated from the actual scatter of the measured ^{3}He count rates (see Fig. 8). This error is included in the error analyses along with the (nonstatistical) single sample error of ±0.4%.

VI. MEASUREMENT PROCEDURES

Five separate measurements of the neutron half-life were made at the rate of about one per month, starting in December 1966. Each measurement was made in a single, continuous run lasting up to 64 hours.

Before and after each run the 4π β spectrometer was calibrated, and the activity of a ^{198}Au source was measured in the spectrometer for comparison with a 4π β-γ measurement.

A cyclic routine for the neutron decay measurements was established. This routine included the four β-spectrum measurement modes (^{6}Li shutter

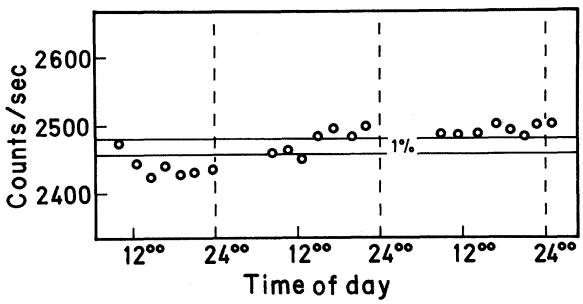

FIG. 8. Fluctuations of the neutron beam density, as periodically measured with the ^{3}He counter during a neutron half-life measurement.

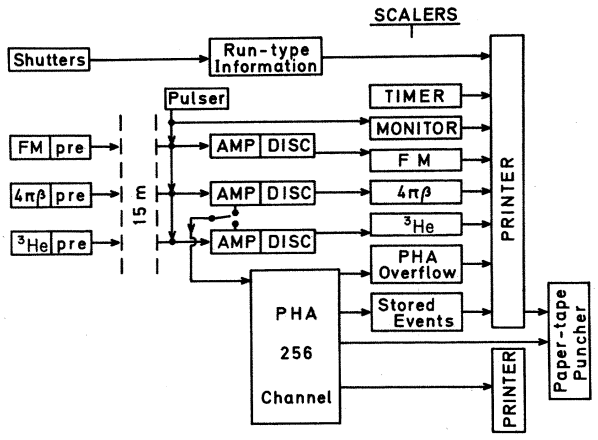

FIG. 9. Block diagram of electronic components.

in or out, Al shutters in or out) and the neutron beam density measurement. Also included was a gain stability check of the β spectrometer with a ^{207}Bi source, and a pulser check of both the β spectrometer and the ^{3}He-counter systems. For every second cycle the order of the modes was reversed.

VII. DATA STORAGE AND REDUCTION

Except for the data storage system, the electronic setup is standard (Fig. 9 shows the block diagram). Pulses from each detector [4π β spectrometer (4π β), ^{3}He counter (He^3), and fission density monitor (FM)] are processed in a preamplifier, and amplifier, and an integral discriminator, and stored in a scaler. Depending on the type of measurement, a 256-channel pulse height analyzer is connected to the relevant amplifier (neutron-density or neutron-decay channel, respectively).

Each neutron half-life run consisted of ~200 individual 10-min measurements (as described in Sec. VI), each of which resulted in a 256-channel spectrum plus scaler readings. Therefore, large amounts of data (~50 000 10-digit figures per run) were obtained and required computer analysis. The data handling system was a relatively elaborate system designed with built-in cross checks. The scalers, shown in Fig. 9, were used only for checking purposes.[15] The data actually used for the half-life determination were the multichannel spectra. All data were stored in two ways: as printed figures and as punched paper tape. Each measurement was identified on the punched tape by a measurement number and information concerning the type of measurement (i.e., which shutters open, ^{3}He counter in or out).

The data tapes were handled in two steps in the computer. The first pass through the computer included cross checks and revealed the runs that contained errors and the type of the errors. Most discrepancies were puncher errors and were easily rectified by comparing punched tapes with numerical printout. Only a small fraction (<5%) of the data were actually rejected. In the second pass the different spectra [A, B, C, D, $A-C$, $B-D$, and $(A-C)-(B-D)$] were summed up from the individual spectra of the complete run. Also, the run was subdivided into single cycles (of one A, B, C, and D spectrum each). For each cycle the relevant difference spectra [$(A-C)$, etc.] were calculated. This was done in order to make statistical checks possible which could indicate the uncertainties obtained and the efficiency of our measuring procedure as far as the elimination of nonstatistical drift in background is concerned.

The scatter of the basic count rate was considerably greater than a statistical expectation (because of drift), whereas the scatter in the differences was reasonable, as expected.

The variation in neutron density was also evaluated (as discussed in Sec. V). From the spectra of the stability runs with the ^{207}Bi source, the gain of the 4π β spectrometer was checked. No large variations were seen ($\ll$1% for a three-day run).

VIII. SUMMARY OF RESULTS

Data obtained in the five measurement runs were treated separately so that each run yielded a value of the neutron half-life. Table V shows the relevant results for these runs and the derivation of the half-life determined from each. The last two long runs (4, 5) are each subdivided into two because of unintended changes in the neutron density. The weighted average of these seven half-life results (T_i) is a half-life of 10.94 ± 0.079 min. The error quoted is a statistical uncertainty (standard deviation σ). It includes all statistical uncertainties: counting statistics, efficiency determination, and filling accuracy of the ^{3}He counter. The quoted value for σ does not include anything about the true scatter of the T_i values, i.e., about the reproducibility. However, if the σ_i values have been judged correctly, the statistical variable $\chi_0^2 = \sum[(T_i - T_{1/2})/\sigma_i]^2$ should have a χ^2 distribution with $(n-1)=6$ degrees of freedom. The value of this variable is calculated to be $\chi_0^2 = 6.5$. The probability that $\chi^2 > \chi_0^2$ is therefore 0.4, which shows good reproducibility and indicates that our judgment about the errors is reasonable.

We categorize the errors according to the following definition: A statistical error need not be a measure of the variation of the associated parameter during a run, but may be an error that is constant during each run and different from run

TABLE V. Results of the separate half-life runs. A figure such as 11.06_{19} means 11.06 ± 0.19, i.e., 19 is the uncertainty (standard deviation) on the last digit.

Run No.	1	2	3	4a	4b	5a	5b
Decay rates in sec^{-1}							
Count rate $(A-C)$ [a]	4.155_{27}	3.544_{29}	3.520_{92}	3.816_{40}	3.960_{31}	4.120_{51}	4.125_{31}
Capture $(B-D)$ [a]	0.193_{31}	0.158_{39}	0.165_{47}	0.247_{40}	0.332_{24}	0.254_{31}	0.307_{32}
$C_d=(A-C)-(B-D)$ [a]	3.962_{33}	3.386_{48}	3.355_{102}	3.569_{70}	3.628_{38}	3.867_{59}	3.818_{46}
Efficiency $\epsilon\Omega$ [b]	0.6800_{68}	0.6800_{68}	0.6800_{68}	0.6800_{68}	0.6800_{68}	0.6800_{68}	0.6800_{68}
Decay rate C_T [c]	5.827_{76}	4.980_{86}	4.634_{148}	5.249_{115}	5.335_{77}	5.687_{104}	5.616_{88}
Neutron density							
Count rate C_n sec^{-1} [a]	2474_6	891_6	855_3	924_{15}	951_4	990_5	1003_4
C_n/n_z [b]	4.717_{28}	1.888_6	1.888_6	1.888_6	1.888_6	1.888_6	1.888_6
Correction f [b]	1.005_3	0.993_3	0.988_3	0.988_{12}	0.988_5	0.988_5	0.988_5
Linear neutron density n_z (n/cm) [c]	525.9_{38}	486.6_{35}	447.3_{21}	483.6_{98}	497.7_{36}	517.9_{40}	524.8_{38}
L (cm)	10.25	10.25	10.25	10.25	10.25	10.25	10.25
$T_{1/2}$ (min) [d]	10.68_{16}	11.13_{21}	11.43_{36}	10.91_{33}	11.04_{18}	10.78_{21}	11.06_{19}
$\Delta\chi^2$ [e]	2.62	0.81	1.84	0.1	0.30	0.57	0.39

[a] Errors were deduced from the scatter of many measurements.
[b] Error estimated for method.
[c] Error evaluated from geometric sum of constituents.
[d] Weighted average of $T_{1/2}=10.94 \pm 0.079$ min.
[e] $\chi_0^2=6.54$, $P(\chi^2>\chi_0^2)=0.4$.

to run (e.g., the statistical part ±1% of the efficiency errors). A systematic error is an error that is the same from run to run. These systematic errors have to be taken into account. The solid-angle error, the capture-γ systematic error, and the systematic error in the efficiency were all considered (discussed earlier in the text) to be corrections, which total up to −3.0%. Thus the half-life shown in Table V is reduced to $T_{1/2} = 10.61 \pm 0.08$ min.

Then the uncertainty part of these same errors and of several others, as reviewed in Table VI, has to be taken into account. If we assume each individual effect in Table VI to be an independent stochastic variable that is described by a Gaussian probability distribution with the average value equal to the correction and the standard deviation equal to the quoted error, and assume that all the parameters are independent, they can be added quadratically. This yields $(-3.0 \pm 1.3)\%$; and, added to the half-life in Table V, we obtain the final result:

$$T_{1/2} = 10.61 \pm 0.16 \text{ min.}$$

IX. CONCLUSION

Our final value for the neutron half-life, 10.61 ±0.16 min, is clearly inconsistent with the value

TABLE VI. Systematic errors to be added to results of Table V.

Parameter x	Value of x used	Systematic error in x	Correction + uncertainty to $T_{1/2}$	Sec.
Effective length L(cm)	10.25	±0.05	±0.5%	III E
Efficiency ϵ	0.6800_{68}	$^{+0.0000}_{-0.0068}$	(+0.5 ± 0.5)%	III B-III C
Solid angle $\Omega/4\pi$	1.000	+0.024 ± 0.006	(−2.4 ± 0.6)%	III D
Neutron density n_z	(Table V)	±0.4%	±0.4%	V
Capture γ B_{cap}	~6% of C_d (Table V)	$^{+0.33\%}_{+1.83\%}$	(−1.1 ± 0.8)%	IV
Total systematic error	(−3.0 ± 1.3)%			
Uncorrected $T_{1/2}$	10.94 ± 0.079 min (Table V)			
Corrected $T_{1/2}$	10.61 ± 0.16 min			

TABLE VII. Comparison of g_A/g_V values.

Present work plus ^{26m}Al data (Refs. 29–31)	-1.239 ± 0.011
Sosnovsky *et al.* plus ^{26m}Al data (Refs. 29–31)	-1.166 ± 0.019
Electron-neutrino correlation, neutron decay (Ref. 32)	-1.22 ± 0.08
Electron neutron-spin correlation, neutron decay (Ref. 33)	-1.26 ± 0.02

11.7 ± 0.3 min measured by Sosnovsky *et al.*[10] (Table I).

Using the ft value of Freeman *et al.*[29] for the decay of ^{26m}Al$(0^+ - 0^+)$ and Blin-Stoyle's method of evaluating g_A/g_V,[30] we obtain

$$g_A/g_V = -1.239 \pm 0.011,$$

which includes radiative corrections. In Table VII, this value is compared with g_A/g_V values from other experiments (Refs. 29–33). There is good agreement with the value obtained from the electron asymmetry in the decay of polarized neutrons.[33]

ACKNOWLEDGMENTS

It is a pleasure to acknowledge the contribution of ideas and the support and encouragement of O. Kofoed-Hansen from the outset of the experiment. We are especially grateful to J. Als-Nielsen for his help with various experimental problems and, in particular, for his contributions to the precision beam density measurements. We thank J. Thomas and L. Løvborg of the Risö Electronics Department for placing at our disposal the absolute 4π β-γ gold-foil coincidence system. We thank S. B. Garfinkel of the U.S. National Bureau of Standards for his cooperation in gold foil calibrations. The excellent technical work of P. Andersen, F. Å. Hansen, B. Kok, and J. Strømstad has made this project possible. We also wish to thank the DR 3 staff for help during the experimental period. One of us (WKB) wishes to express his gratitude for support from the Society of the Sigma Xi through a Grant-in-Aid-of-Research in 1966, and from the Danish Atomic Energy Commission making possible a return to Risö in 1970.

*Present address: Danmarks Ingeniørakademi, Aalborg, Denmark.

†Present address: Danish Space Research Institute, Lyngby, Denmark.

‡Present address: University of Wyoming, Laramie, Wyo.

§Deceased; formerly with Columbia University at Brookhaven National Laboratory, Upton, N. Y.

[1]O. Kofoed-Hansen and C. J. Christensen, *Handbuch der Physik*, edited by S. Flügge (Springer, Berlin, 1962), Vol. XLI, part 2.

[2]R. J. Tayler, Nature 217, 433 (1968).

[3]A. H. Snell and L. C. Miller, Phys. Rev. 74, 1217 (1948).

[4]J. M. Robson, Phys. Rev. 77, 747 (1950).

[5]A. H. Snell, F. Pleasonton, and R. V. McCord, Phys. Rev. 78, 310 (1950).

[6]J. M. Robson, Phys. Rev. 78, 311 (1950).

[7]P. E. Spivak, A. N. Sosnovsky, Y. A. Prokofiev, and V. S. Sokolov, in *Proceedings of the International Conference on the Peaceful Uses of Atomic Energy, Geneva, 1955* (United Nations, New York, 1956), Vol. 2, p. 33.

[8]J. M. Robson, Phys. Rev. 83, 349 (1951).

[9]N. D'Angelo, Phys. Rev. 114, 285 (1959).

[10]A. N. Sosnovsky, P. E. Spivak, Y. A. Prokofiev, I. E. Kutikov, and Y. P. Dobrinin, Nucl. Phys. 10, 395 (1959).

[11]C. J. Christensen, A. Nielsen, A. Bahnsen, W. K. Brown, and B. M. Rustad, Phys. Letters 26B, 11 (1967).

[12]C. J. Christensen, A. Nielsen, A. Bahnsen, W. K. Brown, and B. M. Rustad, Risö Report No. 147, 1967 (unpublished).

[13]B. M. Rustad, J. Als-Nielsen, A. Bahnsen, C. J. Christensen, and A. Nielsen, Rev. Sci. Instr. 36, 48 (1965).

[14]J. Als-Nielsen, A. Bahnsen, and W. K. Brown, Nucl. Instr. Methods 50, 181 (1967).

[15]C. J. Christensen *et al.*, Risö Report No. 226, 1971 (unpublished).

[16]Fabricator: Nuclear Enterprises, Ltd., Bankhead Crossway South, Sighthill, Edinburgh 11, Scotland.

[17]*Tables for the Analysis of Beta Spectra*, National Bureau of Standards Applied Mathematics Series No. 13 (U.S. Government Printing Office, Washington, D. C., 1952).

[18]J. H. Hamilton, R. V. Stockendal, D. C. Camp, L. M. Langer, and D. R. Smith, Nucl. Phys. 36, 567 (1962).

[19]J. Thomas, Risö Report No. 142, 1966 (unpublished).

[20]S. B. Garfinkel (private communication).

[21]J. Als-Nielsen, Nucl. Instr. Methods 50, 191 (1967).

[22]G. Gibson, W. C. Jordan, and E. J. Lauer, Phys. Fluids 6, 116 (1963).

[23]G. Gibson, W. C. Jordan, and E. J. Lauer, Phys. Fluids 6, 133 (1963).

[24]T. K. Fowler, Nucl. Fusion 9, 3 (1969).

[25]D. V. Sivukhin, Rev. Plasma Phys. 1, 1 (1965).

[26]J. Als-Nielsen, Risö Report No. 196, 1969 (unpublished).

[27]J. Als-Nielsen, A. Bahnsen, and W. K. Brown, Risö Report No. 144, 1966 (unpublished).

[28]J. Als-Nielsen and O. Dietrich, Phys. Rev. 133, B925 (1964).

[29]J. M. Freeman, J. G. Jenkin, G. Murray, and D. C.

Robinson, Nucl. Phys. A132, 593 (1969).
[30]R. J. Blin-Stoyle and J. M. Freeman, Nucl. Phys. A150, 369 (1970).
[31]H. Bühring and H. Schopper, Kernforschungszentrum, Karlsruhe Report No. KFK-307, 1965 (unpublished).
[32]V. V. Vladimirsky, V. K. Grigorev, V. A. Ergakov, D. P. Zharkov, and Y. V. Trebukhovsky, Izv. Akad. Nauk SSSR, Ser. Fiz. 25, 1121 (1961) [Bull. Acad. Sci. U.S.S.R., Phys. Ser. 25, 1128 (1961)].
[33]C. J. Christensen, V. E. Krohn, and G. R. Ringo, Phys. Rev. C 1, 1693 (1970).

PHYSICAL REVIEW D VOLUME 5, NUMBER 7 1 APRIL 1972

Total Hadronic Cross Section of γ Rays in Hydrogen in the Energy Range 0.265–4.215 GeV

T. A. Armstrong, W. R. Hogg, G. M. Lewis, and A. W. Robertson
Department of Natural Philosophy, The University, Glasgow, Scotland

and

G. R. Brookes, A. S. Clough,* J. H. Freeland, W. Galbraith, and A. F. King
Department of Physics, The University, Sheffield, Yorkshire, England

and

W. R. Rawlinson, N. R. S. Tait, J. C. Thompson, and D. W. L. Tolfree
Daresbury Nuclear Physics Laboratory, Daresbury, Cheshire, England
(Received 30 November 1971)

The total cross section of γ rays in hydrogen resulting in hadron production, σ_T, has been measured over the energy range 265–4215 MeV. A tagging system with narrow energy bins was employed. Structure in the resonance region followed by a steady fall with energy has been observed and the results are analyzed. The forward amplitude of γ-proton scattering is evaluated, and its behavior in the Argand diagram studied as a function of energy. The relationships of the measurements to Regge-pole theory and the vector-dominance model are detailed.

I. INTRODUCTION

Total cross sections for long-lived strongly interacting particles can generally be determined by absorption methods. Good data on these, over a wide energy band, have therefore been accumulating for some time.

A measurement of the total cross section for γ rays, σ_T, involving strong-interaction vertices has, however, to be made in a different way because this γ-ray cross section is dwarfed by those of the prolific purely electromagnetic processes. Also γ rays are generally available, at high energies, only as the broad and steeply changing bremsstrahlung spectrum, making monochromatic studies very difficult.

At the time this experiment was started little direct data existed as a function of energy. Recourse had generally to be made to a compilation of the separate processes where known, the contribution of each being roughly assessed from often sparse differential cross-section data. Additional information came from bubble-chamber work, particularly that using monochromatic beams.[1]

Quite recently the situation has changed in a number of ways. A study of inelastic electron scattering at SLAC,[2] for various squared four-momentum transfers q^2 of the virtual photon, led to an extrapolation to $q^2=0$, providing an indirect assessment of σ_T for real photons. Direct measurements of σ_T have now also been reported, in several energy bands.

These direct investigations measure the production rates of hadronic events, and successfully reject the vastly preponderant electromagnetic events by an angular separation. The use of a tagging system enables the energy of the incident γ ray responsible for an observed hadronic event to be identified. As compensation for the trouble of setting up such a system the bremsstrahlung spectrum can be then turned to good use; it enables the energy dependence of σ_T to be displayed over a wide range of energy values in a single experimental run.